The Astrophysical Journal, 806:178 (12pp), 2015 June 20 doi:10.1088/0004-637X/806/2/178

EXPLORING STELLAR EVOLUTION MODELS OF sdB STARS USING MESA

Jan-Torge Schindler, Elizabeth M. Green, and W. David Arnett
Steward Observatory, University of Arizona, 933 North Cherry Avenue, Tucson, AZ 85721, USA
Received 2014 October 29; accepted 2015 May 9; published 2015 June 17

ABSTRACT

Stellar evolution calculations have had great success reproducing the observed atmospheric properties of different classes of stars. Recent detections of *g*-mode pulsations in evolved He burning stars allow a rare comparison of their internal structure with stellar models. Asteroseismology of subdwarf B (sdB) stars suggests convective cores of 0.22–0.28 $M_{\odot}$, $\gtrsim$45% of the total stellar mass. Previous studies found significantly smaller convective core masses ($\lesssim$0.19 $M_{\odot}$) at a comparable evolutionary stage. We evolved stellar models with Modules for Experiments in Stellar Astrophysics (MESA) to explore how well the interior structures inferred from asteroseismology can be reproduced by standard algorithms. Our qualitative evolutionary paths, position in the $\log g - T_{\rm eff}$ diagram, and model timescales are consistent with previous results. The sdB masses from our full evolutionary sequences fall within the range of the empirical sdB mass distribution, but are nearly always lower than the median. Using standard MLT with atomic diffusion we find convective core masses of ~0.17–0.18 $M_{\odot}$, averaged over the entire sdB lifetime. We can increase the convective core sizes to be as large as those inferred from asteroseismology, but only for extreme values of the overshoot parameter (overshoot gives numerically unstable and physically unrealistic behavior at the boundary). High resolution three-dimensional simulations of turbulent convection in stars suggest that the Schwarzschild criterion for convective mixing systematically *underestimates the actual extent of mixing because a boundary layer forms.* Accounting for this would decrease the errors in both sdB total and convective core masses.

Key words: convection – stars: interiors – subdwarf

1. INTRODUCTION

With the increasing improvement of stellar observations and the introduction of new types of observations, it has become possible to constrain the processes involved and test the validity of the underlying physics. Here we focus specifically on subdwarf B (sdB) stars which have been detected to have *g*-mode pulsations, and we use the Modules for Experiments in Stellar Astrophysics (MESA) code (Paxton et al. 2011, 2013) for comparison with observational constraints, with particular emphasis on mixing in the deep interior, a major unsolved problem in stellar evolution.

1.1. sdB Stars—General Introduction and Observational Results

sdB stars are hot ($T_{\rm eff}$ = 20,000–40,000 K) and compact ($\log g$ = 5.0–6.2) stars that are found in all stellar populations of our own Galaxy as well as in other old galaxies. Located on the extreme horizontal branch (EHB), they are understood to be helium burning objects with very thin hydrogen envelopes ($M_{\rm H} < 0.01\ M_{\odot}$; Heber 1986; Saffer et al. 1994). While it is well known that they will directly evolve to become white dwarfs once their central helium is exhausted, the details and the relative importance of the various evolutionary channels leading to the EHB are still poorly understood. Numerous single and binary star scenarios have been proposed (Mengel et al. 1976; Castellani & Castellani 1993; D'Cruz et al. 1996; Han et al. 2002, 2003; Miller Bertolami et al. 2008).

Many sdB stars exhibit stellar pulsations, the shorter (100–400 s) pressure(*p*)-mode pulsations found in hotter V361 Hya stars (Kilkenny et al. 1997) and the longer (2000–14000 s or longer) gravity(*g*)-mode pulsations in cooler V1093 Her stars (Green et al. 2003), or both, in hybrid pulsators called DW Lyn stars (Schuh et al. 2006).

Detailed work has recently been done to reproduce the observed pulsational properties of sdB stars with stellar evolution models. It has been shown that time-dependent diffusive processes, including mass loss, gravitational settling, and radiative levitation (Chayer et al. 2004; Fontaine et al. 2006a; Michaud et al. 2007, 2008; Hu et al. 2009, 2011) are important for recovering the iron-group opacity bump that excites the pulsations (Charpinet et al. 1997) in these stars, as well as the correct position of the instability strip in the $\log g - T_{\rm eff}$ diagram (Fontaine et al. 2006b; Hu et al. 2008, 2009, 2010, 2011; Bloemen et al. 2014).

Pulsational frequencies derived from light curves of *p*- and *g*-mode sdB pulsators using ground-based as well as space-borne (e.g., CoRoT and *Kepler*) instruments have been analyzed by asteroseismology. Using the forward method (e.g., Charpinet et al. 2008; Van Grootel et al. 2008), the parameters derived by asteroseismology, in particular total stellar masses, surface gravities and effective temperatures, agree remarkably well with measurements from other techniques such as light curve modeling of eclipsing binary systems and spectroscopic analyses (Green et al. 2011, Table 3; Van Grootel et al. 2013).

Asteroseismology of *g*-mode pulsators also provides observational benchmarks for the inner structure of those stars, e.g., the extent of the inner convection zone and the nature of the abundance gradient above the boundary. Van Grootel et al. (2010a, 2010b) and Charpinet et al. (2011b) recently derived sdB He–CO convective core masses for the first time from asteroseismology of three *g*-mode pulsators: $M_{\rm cc} = 0.22 \pm 0.01\ M_{\odot}$, $M_{\rm cc} = 0.28 \pm 0.01\ M_{\odot}$, and either $M_{\rm cc} = 0.274^{+0.008}_{-0.010}\ M_{\odot}$ or $M_{\rm cc} = 0.225^{+0.011}_{-0.016}\ M_{\odot}$.[1] All three

[1] The asteroseismological analysis of Charpinet et al. (2011b) identified two equally probable solutions.

stars were determined to be significantly less than halfway through their He-burning lifetimes, having consumed only about 20%–40% of the helium fuel in their cores.

Standard stellar evolution, without any additional mixing at the boundary of the convective core, predicts a constant convective core mass of $\sim 0.1\ M_{\odot}$ for these stars. When some form of overshoot and semiconvection (Sweigart 1987), partial mixing (Dorman & Rood 1993) or atomic diffusion (Michaud et al. 2007) is included,[2] the models produce growing convective cores, with masses up to $M_{cc} \sim 0.17$–$0.19\ M_{\odot}$ at an evolutionary stage comparable to the sdB stars whose convective cores were inferred from asteroseismology. Sweigart and Dorman achieved semiconvective or partially mixed cores that extended up to $\sim 0.25\ M_{\odot}$ by the end of the He core burning lifetime, but the observations indicate that such large cores are achieved much earlier.

The forward modeling method implemented by both Van Grootel and Charpinet to analyze sdB asteroseismic data uses static stellar models covering a much larger range of parameter space than theoretical models that are constrained to lie along evolutionary tracks. Since their results are independent of evolutionary calculations, this allows us to test various physics options in a state-of-the-art stellar evolution code (MESA).

For this paper, we calculated a series of sdB stellar evolution models to compare with observational results derived from both spectroscopy and asteroseismology. In Section 2, we explain the method and assumptions in our stellar evolution calculations. In Section 3, we present our results, discuss the agreement with atmospheric parameters derived from spectroscopic observations and compare with previous sdB models. Section 4 focuses on the convective cores of sdB stars and the effects of different input physics on the extent of the inner convection zone and the convective core evolution. We summarize our findings in Section 5.

1.2. Mixing Processes

Turbulent convection is an essential process of energy transport in stars. Macroscopic mass elements start to rise (or sink) in dynamically unstable regions, delivering their excess (or deficit) of heat to cooler (or hotter) layers and thus transport energy and material throughout the star. This is a non-linear process governed by the Navier–Stokes equation, and occurs on the dynamical timescale.

1.2.1. Canonical Mixing

MESA treats the mixing of convective elements as a "diffusive" process, as do most stellar evolution codes. This "diffusion" operator is chosen for mathematical convenience (Eggleton 1972), based on parameters estimated from the mixing length theory (Böhm-Vitense 1958) as formulated by Cox & Giuli (1968).

To estimate the extent of dynamically unstable regions, two criteria of linear stability are implemented in MESA. The standard Schwarzschild criterion for instability,

$$\nabla_{\rm rad} > \nabla_{\rm ad} \tag{1}$$

and the Ledoux criterion, taking radial composition gradients ∇_{μ} into account,

$$\nabla_{\rm rad} > \nabla_{\rm ad} + \frac{\phi}{\delta}\nabla_{\mu}, \tag{2}$$

where

$$\phi := \left(\frac{\partial \ln \rho}{\partial \ln \mu}\right)\Bigg|_{P,\mu} \quad \delta := -\left(\frac{\partial \ln \rho}{\partial \ln T}\right)\Bigg|_{P,T}. \tag{3}$$

Historically, convective mixing was supposed to occur in the region in which the Schwarzschild condition (Equation (1)) was violated; we will call this *canonical mixing*. In addition to this canonical mixing, it has proven desirable to consider additional mixing processes (some of which are not truly different, but overlooked in the stellar approximation to turbulent hydrodynamics).

1.2.2. Overshoot

The term *overshoot* refers to the transport of energy and material across the boundary from the dynamically unstable region into the dynamically stable region. The additional mixing is calculated using the diffusion coefficient from the previous MLT calculations near the boundary layer and extrapolates it into the radiative region with an exponential decay, following Herwig (2000); this procedure is based on simulations of fluids in shallow convection zones, of homogeneous composition (Freytag et al. 1996). It has no compositional dependence. The additional term is referred to as the overshoot mixing diffusion coefficient,

$$D_{\rm OV} = D_{\rm conv,0} \exp\left(-\frac{2\Delta r}{f_{\rm ov}\,\lambda_{P,0}}\right) \tag{4}$$

where $D_{\rm conv,0}$ is the previously calculated diffusion coefficient at a user defined location close to the Schwarzschild boundary, $\lambda_{P,0}$ is the local pressure scale height, and Δr is the distance of overshoot into the radiative layer. The local pressure scale height is the exponential attenuation length for g-mode waves (Landau & Lifshitz 1987), and it is assumed that overshoot falls off as wave energy. The free parameter $f_{\rm ov}$ sets the extent of the overshooting region and needs to be adjusted by the user depending on the problem.

In Paxton et al. (2013) an $f_{\rm ov}$-parameter of $f_{\rm ov} = 0.004$–0.015 was used to calculate models of a non-rotating $1.5\ M_{\odot}$ star. Herwig (2000) used an overshoot parameter of $f_{\rm ov} = 0.016$ for his study of $3\ M_{\odot}$ and $4\ M_{\odot}$ asymptotic giant branch (AGB) stars.

1.3. Atomic Diffusion and Radiative Levitation

Georges Michaud led in the application of true *diffusion* processes and radiative levitation to stellar evolution models (Michaud 1970, 1991). These processes have been applied to horizontal branch (HB) and sdB stars by Michaud et al. (1985), Bergeron et al. (1988), Fontaine & Chayer (1997), Fontaine et al. (2003, 2006a, 2006b), Chayer et al. (2004), Michaud et al. (2007, 2008, 2011), Hu et al. (2008, 2009, 2010, 2011), Bloemen et al. (2014).

Hu et al. (2011) defined atomic diffusion to include gravitational settling, thermal diffusion, concentration

[2] We note that atomic diffusion is physically well-defined, while overshoot and mixing are approximations to assumed fluid flow behavior, and are therefore likely to be more uncertain.

Table 1
Specified Physics for Standard Set of Stellar Evolution Models

Opacity	OPAL type II electron conduction
Nuclear network	`pp_cno_extras_o18_ne22.net`
Metallicity	$Z = 0.02$
Composition	$Y = 0.30$, $X = 0.68$
MLT	$\alpha_{\rm MLT} = 2$
RGB wind scheme	$\eta_{\rm Reimers} = 0.5$
AGB wind scheme	$\eta_{\rm Blöcker} = 0.5$
Convection criterion	Schwarzschild
Diffusion options	Atomic diffusion

diffusion, and radiative levitation. Atomic diffusion in MESA includes all of these processes except radiative leviation, which is a separate option. Gravitational settling and radiative levitation are particularly important to recover the iron-group opacity bump that excites the pulsations in these stars (Charpinet et al. 1997), the correct position of the instability strip in the $\log g - T_{\rm eff}$ diagram (Bloemen et al. 2014), and help in understanding their observed atmospheric abundances (Michaud et al. 2011). We will further examine the effects of atomic diffusion on the deep interior in Section 4.

2. STELLAR EVOLUTION CALCULATIONS

2.1. sdB Modeling Using MESA

The stellar evolution calculations were done with version 7184 of MESA (Paxton et al. 2011, 2013) in order to extend the results of Østensen et al. (2012). MESA offers a variety of up-to-date physics modules, including several MLT convection options, and is capable of evolving stars through the He-flash, a crucial part of the evolutionary path to sdB stars. The latter is modeled as a quasi-static process, with MLT mixing, as a substitute for the full dynamical process.

Because our main goal was to devise a simple model that allowed us to focus on the inner convection zone of the star, we used standard values and descriptions for the input physics, varying the defaults for consistency with the observational data, as described below.

The physics options adopted for our standard models are summarized in Table 1. They include an atmospheric boundary condition of $\tau = 2/3$ and a mixing length parameter of $\alpha_{\rm MLT} = 2$. We further selected a nuclear network designed to include all reactions for hydrogen and helium burning. Representative abundances of $Z = 0.02$, $Y = 0.28$, and $X = 0.70$ were adopted, because most well-studied (i.e., nearby) sdB stars belong to the field population of the galactic disk (Saffer 1991; Saffer et al. 1994), and the few that are found in old open clusters (where their progenitors' abundances can be measured) appear to be preferentially metal-rich (see Section 3.3). We used the Reimers wind scheme (Reimers 1975) with $\eta_{\rm Reimers} = 0.5$ on the red giant branch (RGB). For the post-EHB phase we used the Blöcker wind scheme (Blöcker 1995) with $\eta_{\rm Blöcker} = 0.5$.

MESA offers the opacity tables of Iglesias & Rogers (1993, 1996) and includes their OPAL type I opacity tables with fixed metal distributions as the default option. However, the interior abundances of carbon and oxygen in sdB stars change enough to modify the opacity, not only during He burning on the EHB, but also during their prior evolution, in particular during the He flash and the subsequent transition to the ZAEHB. It is therefore necessary to use the OPAL type II opacity tables which allow for time dependent variation of the C and O abundances.

MESA includes electron conduction opacities (Cassisi et al. 2007) as the default case. Electron conduction becomes the dominant energy transport mechanism in significantly degenerate stellar cores and is thus required for our study.

Mixing due to atomic diffusion has been traditionally assumed to be small during stellar evolution, but it is necessary to obtain the correct structure to excite pulsations in sdB stars and reproduce the observed instability strips (Fontaine et al. 2003, 2006a, 2006b; Hu et al. 2009, 2011; Bloemen et al. 2014). As chemical diffusion smoothes out abundance gradients at the boundary of the convective core, this diffusion, combined with time dependent opacities, allows the convective core to grow during the sdB evolution. This was first noted by Michaud et al. (2007) in the context of somewhat more massive, but essentially similar, HB stars.

Hence we included type II opacities as well as atomic diffusion processes in all of our stellar evolution calculations, unless otherwise specified. We deliberately did not include radiative levitation in our set of standard parameters since it is computationally very expensive and has little to no effect on the interior mixing regions of the sdB models (see Section 4).

MESA calculates the enthalpy flux from standard mixing length theory (Cox & Giuli 1968), using either the Schwarzschild or Ledoux stability criterion. With the latter, semiconvection may be included (Langer et al. 1983). Our initial investigation of the effects of semiconvection on the convective cores of sdB stars showed that semiconvection, as implemented in MESA, has little effect on the convective core sizes. The Ledoux criterion with maximal semiconvection gives convective core sizes similar to those obtained with the Schwarzschild criterion. Convective overshoot is implemented according to Herwig (2000). In Section 4, we investigate the effect of varying amounts of overshoot on the convective cores.

2.2. Our Method

We modeled sdB stars that have evolved from solar type stars in binary systems through the common envelope or the Roche lobe overflow channel (Han et al. 2002). These apparently very common scenarios are believed to occur in binary systems where the companion strips away the hydrogen envelope of the expanding progenitor star as the latter evolves toward the tip of the RGB. When most of the red giant envelope is removed, hydrogen shell burning is quenched, the He-core stops growing, and the star begins to contract away from the RGB. If the helium core is sufficiently massive for the contraction to trigger helium ignition, the star will evolve onto the EHB and begin burning He in its core as an sdB star.

For simplicity, we simulated the effect of binary mass stripping by removing the envelopes of non-rotating single stars. Both spectroscopy (e.g., Heber et al. 2000) and asteroseismology (e.g., Randall et al. 2007; Baran et al. 2012) indicate that sdB stars are generally slow rotators, except those that have been spun up to some degree by a binary companion. Our assumption that rotation does not play an important role even in the interiors of sdB stars is based on available asteroseismic evidence, which suggests rigid rotation in both binary and single sdB stars for the few cases so far in

which the interior rotation could be constrained (Charpinet et al. 2008, 2011a; Van Grootel et al. 2008; Pablo et al. 2012).

Our first step was to create pre-main-sequence (PMS) models, which are specified by their initial mass $M_{\rm ini}$, a uniform composition, a luminosity and a central temperature ($T_{\rm c} = 9 \times 10^5$ K by default). Once the PMS routine found the central density $\rho_{\rm c}$ that gives the model the desired mass, we evolved the star up to the point of the He-flash. Just before the flash occurred, we saved the structure as our sdB progenitor model. Our procedure provides an *upper* limit to the He core mass of the resulting sdB star, since the progenitor could have been stripped prior to the He flash when the He core mass was up to $\sim$0.02 $M_\odot$ smaller and it would still have evolved onto the EHB (Castellani & Castellani 1993; D'Cruz et al. 1996).

For the next step, we stripped away mass from the sdB progenitor model beginning with the outermost cell using the `relax_mass` option of MESA. This option ensures that the mass of the star is adjusted to the specified value of `new_mass`. The mass loss occurs in a series of small episodes until the requested new mass is reached. Then the code begins the actual stellar evolution toward the zero-age EHB (ZAEHB). Mass loss continues to occur between the RGB tip and the ZAEHB. Using this method, we reduced the hydrogen envelope down to typical values for sdB stars in the range of $M_{\rm H} = 10^{-4}$–10^{-3} $M_\odot$.

This simple mass loss procedure differs from the real dynamics in that it is modeled as a quasi-static process. The full 3D well-resolved hydrodynamics for a binary star over evolutionary timescales is still beyond the capability of modern computation. Therefore, following Dorman et al. (1993), Hu et al. (2009, 2011), Østensen et al. (2012), and Bloemen et al. (2014), we adopted a more tractable approach.

The evolutionary tracks of sdB stars are primarily influenced by two factors: the mass of the He core after the envelope has been stripped and the amount of remaining hydrogen envelope. As seen in previous studies (Dorman et al. 1993; Han et al. 2002), the initial mass of the progenitor star, $M_{\rm ini}$, determines the mass of the He core at the He flash and therefore the approximate total mass of our sdB stars, subject to a very small dependence on composition. For ages appropriate for old disk stars ($\lesssim$10 Gyr), the more massive the progenitor star, the earlier the star begins helium fusion and thus the less massive the He core. For a given He core mass, the tiny envelope mass is decided by the parameter $M_{\rm new}$, the new stellar mass after stripping off the envelope. Qualitatively speaking, the more massive the sdB envelope, the lower the effective temperature and the surface gravity. In our survey set of calculations, we varied the initial mass, $M_{\rm ini}$, between 1.0 and 2.5 $M_\odot$ and the new mass parameter, $M_{\rm new}$, between 0.472 and 0.490 $M_\odot$.

3. sdB MODELS WITH CANONICAL MIXING AND ATOMIC DIFFUSION

In this section we compare the results of our sdB modeling with observational data and with other stellar evolution calculations. We created a range of sdB models using standard MLT (i.e., excluding overshoot and semiconvection) and the Schwarzschild criterion to explore the effects of varying the initial mass, $M_{\rm ini}$, and stripped mass, $M_{\rm new}$, on our sdB models.

We show that our models are quite consistent with previous calculations of sdB stars.

The distances to field sdB stars are only approximate, so luminosities cannot be accurately calculated. However, since effective temperatures and surface gravities can be inferred from a variety of methods and the masses of most sdB stars are very similar, they are typically plotted in the $\log g - T_{\rm eff}$ plane instead of an HR diagram.

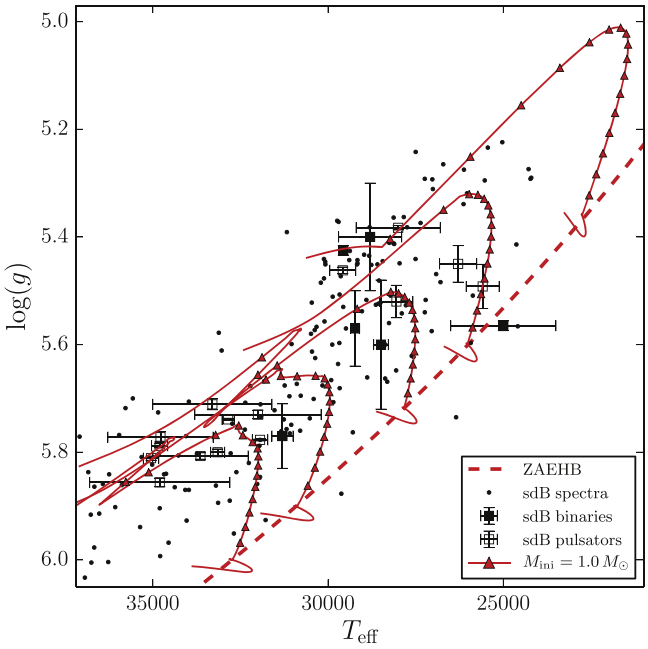

Figure 1. Evolutionary tracks of sdB stars in the $\log g - T_{\rm eff}$ diagram. The solid black curves (red in the online journal) show the evolutionary tracks of our models with $M_{\rm ini} = 1.0\,M_\odot$ and $M_{\rm sdB} = 0.4652$, 0.4654, 0.4658, 0.4669, 0.4705 $M_\odot$ from bottom to top. The black (red) triangles intersect the lines in intervals of 10^7 years, depicting the region where most sdB stars should be found. The small loop at the bottom of each track shows the final approach to the ZAEHB. The dashed lines show the ZAEHB's for our evolutionary models of $M_{\rm ini} = 1.0\,M_\odot$. The spectroscopic data points (small black dots) for sdB stars (Green et al. 2008) agree very well with the open and filled squares with error bars derived from eclipsing binary and asteroseismology analyses, respectively (Fontaine et al. 2012).

Figure 1 shows the ZAEHB (lower dashed line) and evolutionary tracks (solid lines) for our set of sdB models with $M_{\rm ini} = 1.0$ and a range of $M_{\rm new}$. The tracks cover only the period of helium core burning, when the star is characterized as an sdB star. For comparison, we plot observed spectroscopic data derived with the use of NLTE model atmospheres (Green et al. 2008), along with results from binary modeling and asteroseismology (Fontaine et al. 2012). (Although Fontaine listed spectroscopic values for the effective temperatures, because they are poorly constrained by asteroseismology, we show the asteroseismic values for $T_{\rm eff}$ whenever they were available.)

Our models reproduce the characteristic hook-shaped sdB evolutionary tracks, corresponding to stable helium core burning, as well as the shape of the ZAEHB. The tracks overlap the distribution of the observational data points fairly well, except for a small overall shift toward lower $T_{\rm eff}$ and/or higher $\log g$.

Figure 2 shows the ZAEHB (lower dashed line) and the corresponding tracks (solid lines) for a different sequence of sdB models evolved from an initial mass of 2.0 $M_\odot$. The resulting He core masses, and therefore the total sdB masses, are about 0.03 $M_\odot$ smaller than in the case of the 1.0 $M_\odot$ progenitor. The ZAEHB for the 1.0 $M_\odot$ progenitor sequence of Figure 1 is shown (upper dashed line) for comparison.

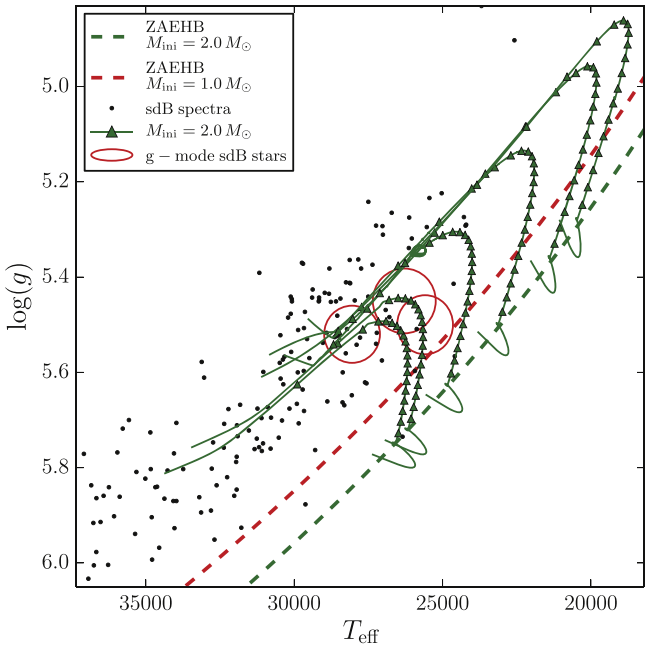

Figure 2. Evolutionary tracks of sdB stars in the $\log g - T_{\rm eff}$ diagram. The solid black curves (green in the online journal) show the evolutionary tracks for sdB stars with $M_{\rm ini} = 2.0\,M_\odot$ and $M_{\rm sdB} = 0.4357$, 0.4363, 0.4373, 0.4389, 0.4415, 0.4433 $M_\odot$. The dashed lines show the ZAEHB for $M_{\rm ini} = 1.0\,M_\odot$ (upper/red) and $2.0\,M_\odot$ (lower/green). The smaller He core masses developed by the more massive progenitors shift the ZAEHB for the $M_{\rm ini} = 2.0\,M_\odot$ models toward lower $T_{\rm eff}$/higher $\log g$ relative to the ZAEHB for $M_{\rm ini} = 1.0\,M_\odot$. The observed spectroscopic data points (black dots) are the same as in Figure 1. The large open ellipses (black/red) correspond to the three g-mode sdB stars analyzed with asteroseismology, whose total masses are 0.496, 0.471, and 0.463/0.452 $M_\odot$ (from left to right).

It is also apparent from Figure 2 that the three g-mode sdB stars whose convective core masses were derived from asteroseismology (plotted as open ellipses) have not evolved very far from the ZAEHB's appropriate for their masses.

Details for the sequences of evolutionary tracks in Figures 1 and 2 are given in Table 2. The average sdB mass, the total mass of hydrogen (essentially all in the envelope), and the extent of the inner convection zone of the sdB star are averaged over the time of helium core burning (the sdB lifetime). We also provided the ZAEHB core and envelope masses for all stellar models.

In agreement with previous HB/EHB stellar models, a smaller He core mass with the same set of envelope masses shifts the ZAEHB in the direction of lower effective temperatures and slightly higher surface gravities, whereas a different envelope mass for the same core mass slides the starting point of the sdB track up or down along the ZAEHB. Therefore, mass loss between the He flash and the ZAEHB results in hotter, higher-gravity sdB tracks, but the position of the ZAEHB does not change.

We ran additional sets of simulations for sdB stars with $M_{\rm ini} = 2.3$ and $2.5\,M_\odot$ progenitors (not shown). Their helium core masses are even less massive and thus the ZAEHB and sdB evolutionary tracks are further shifted to even lower temperatures/higher gravities. In these models the helium core mass is so low that the stars start helium fusion before the material in the helium core becomes degenerate.

3.1. Comparison with Other Evolutionary Models and Observations

We compared our results with older evolutionary tracks computed by Dorman for Charpinet et al. (2000, 2002), and with recent work by Østensen et al. (2012), Bloemen et al. (2014), and G. Fontaine (2015, private communication).

Dorman's primary set of models (Charpinet et al. 2002) adopted a He core mass of 0.4758 $M_\odot$. We could not achieve that high of an evolutionary core mass with our standard set of parameters for the same solar composition. Therefore, we used MESA to construct a new ZAEHB, starting from a He main-sequence star with a 0.4758 $M_\odot$ core mass and using OPAL type II opacities. Figure 3 shows that this ZAEHB is completely consistent with the starting points of Dorman's sdB tracks. Our model sdB tracks from Figure 1 ($M_{\rm ini} = 1.0\,M_\odot$) also agree well with Dorman's, spanning essentially the same range in $\log g - T_{\rm eff}$ space, although ours are slightly shifted to lower temperatures and gravities due to $\sim$0.01 $M_\odot$ smaller He cores.

For a further comparison, we constructed two ZAEHBs from a He main-sequence star with a core mass of 0.47 $M_\odot$ using type I opacities as well as type II. Type II opacities differ from type I because of the composition change of C and O during thermonuclear evolution. It is evident from Figure 3 that type I opacities shift the evolutionary tracks away from the distribution of observed sdB stars. The significant size of this effect indicates the importance of the opacities for the position of the ZAEHB.

Our use of OPAL type II opacities, instead of the MESA default type I opacities, appears to be the main reason why our EHB evolutionary tracks agree more closely with the observed points than those of Østensen et al. (2012).

The 0.47 $M_\odot$ core mass, type II ZAEHB we constructed was also found to be essentially identical with the ZAEHB derived by Fontaine and collaborators from static models having the same core mass (G. Fontaine 2015, private communication). Their models include radiative levitation as well as gravitational settling, and use opacities equivalent to OPAL type II in MESA.

In Figure 4, we compare our sdB models from Figure 1 to models by Bloemen et al. (2014). We chose a subset of their models that have sdB masses closest to our models. Theirs all have a total sdB mass of 0.47 $M_\odot$ with slightly different He core masses of $M_{\rm He\text{-}core} = 0.4699$, 0.4698, 0.4693, 0.4678 $M_\odot$ (from bottom to top). Since Hu et al. (2011) and Bloemen et al. (2014) focused on the pulsational properties of the sdB stars, they specifically included radiative levitation in order to recover the iron-group opacity bump. They used opacities from the Opacity Project (Badnell et al. 2005), which are independent of OPAL type II opacities.

Bloemen et al.'s evolutionary tracks agree remarkably well with our tracks computed without radiative levitation, indicating that this process has little effect on the shapes or the position in the $\log g - T_{\rm eff}$ diagram.

We conclude that MESA models with our standard set of input parameters (Table 1), are therefore quite capable of reproducing the ZAEHB and evolutionary tracks of sdB stars derived using other stellar codes, as long as the He core masses and opacities are essentially the same. The small offset of our sdB tracks relative to the observational points in Figure 1 could therefore be due to either the evolutionary He core masses or the opacities.

Table 2
Properties for sdB Tracks in Figure 1 with $M_{ini} = 1.0$ (Upper Section) and in Figure 2 with $M_{ini} = 2.0$ (Lower Section)

New Mass $M_{new}(M_\odot)$	ZAEHB Core Mass $(M_\odot)$	ZAEHB Envelope Mass $(10^{-3}\,M_\odot)$	Average sdB Mass $M_{sdB}(M_\odot)$	Average sdB Hydrogen Mass $M_{H1}(10^{-3}\,M_\odot)$	sdB Lifetime (10^6 years)	Average Convective Core Mass $M_{cc}(M_\odot)$
0.4720	0.4596	5.722[a]	0.4652	0.23	160.7	0.181
0.4730	0.4630	2.451[a]	0.4654	0.25	148.9	0.179
0.4740	0.4650	0.676	0.4656	0.25	160.9	0.179
0.4750	0.4651	0.758	0.4658	0.30	162.2	0.179
0.4760	0.4652	0.903	0.4660	0.41	142.6	0.173
0.4800	0.4652	1.813	0.4669	0.95	146.8	0.172
0.4850	0.4650	5.780	0.4705	3.46	171.3	0.173
0.4900	0.4648	10.365	0.4749	6.27	174.4	0.170
0.4360	0.4350	0.772	0.4357	0.34	193.3	0.161
0.4380	0.4354	0.978	0.4363	0.46	194.3	0.161
0.4420	0.4356	1.809	0.4373	0.99	201.3	0.161
0.4450	0.4355	3.595	0.4389	2.11	220.5	0.163
0.4480	0.4354	6.328	0.4415	3.86	227.0	0.161
0.4500	0.4353	8.208	0.4433	5.03	226.3	0.159

Note.
[a] During the He flash hydrogen is mixed down in these two models, which gives larger envelope masses due to our envelope definition ($X_H > 0.1$). The pre-flash envelope masses are $0.468 \cdot 10^{-3}\,M_\odot$ for the first and $0.505 \cdot 10^{-3}\,M_\odot$ for the second model.

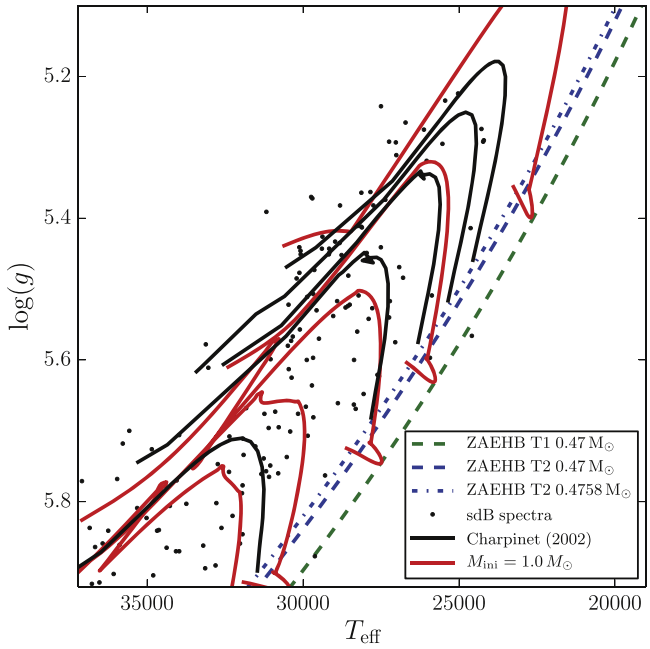

Figure 3. We compare evolutionary tracks (black solid curves) calculated by Ben Dorman with $M_{He\text{-}core} = 0.4758\,M_\odot$ (Charpinet et al. 2002) with a MESA ZAEHB constructed using the same He-core mass and OPAL type II opacities (dotted–dashed line; blue in the online journal). The latter agrees remarkably well with the starting points of Dorman's tracks. For comparison, we show our evolutionary tracks from Figure 1 (gray/red solid lines; OPAL II opacities). We also display two MESA ZAEHB's for $M_{He\text{-}core} = 0.47\,M_\odot$, close to the mean of the empirical mass distribution of sdB stars Fontaine et al. (2012); the gray (green) lower dashed line was constructed with OPAL I opacities and the black (blue) dashed line with OPAL II opacities. The spectroscopic data points (dots) are the same as in Figure 1.

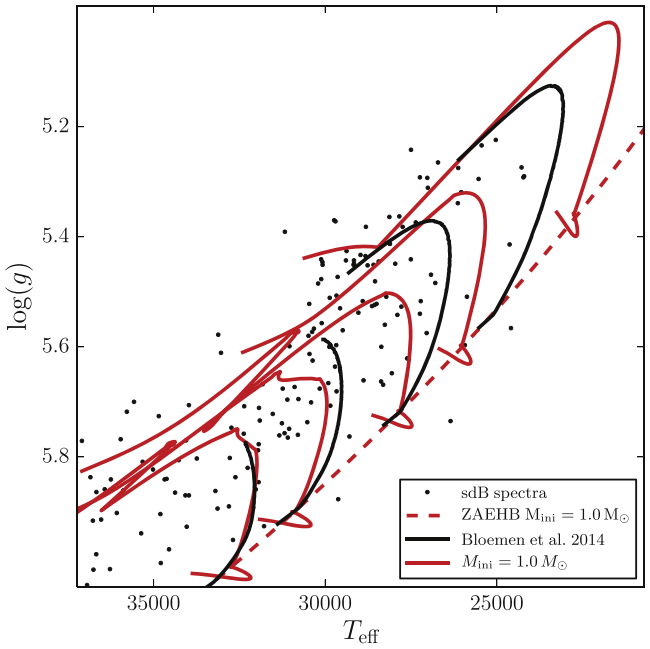

Figure 4. We compare our evolutionary tracks (gray; red in the online journal) and the corresponding ZAEHB (dashed gray/red) from Figure 1 with selected stellar models from Bloemen et al. (2014) having a total mass of $M_{sdB} = 0.47\,M_\odot$ and helium core masses at the ZAEHB of $M_{He\text{-}core} = 0.4699, 0.4698, 0.4693, 0.4678\,M_\odot$ (from bottom to top). The spectroscopic data points (dots) are the same as in Figure 1.

The canonical timescale for the sdB lifetime is about 100 Myr (Dorman et al. 1993; Charpinet et al. 2000). We calculated sdB lifetimes of approximately 140–170 Myr for $M_{ini} = 1.0\,M_\odot$ (top part of Table 2), in fair agreement with the earlier values, and in very good agreement with Bloemen et al. (2014), who found lifetimes of approximately 183, 180, 149, and 122 Myr (from bottom to top) for the four models shown in Figure 4. We note that the lifetimes in our simulations are not monotonic functions of mass, but depend upon details of the mixing algorithms, which seem to be very sensitive to the initial conditions (see Section 4). The smoothest evolutionary tracks are those in which mixing is dominated by atomic diffusion.

Table 3
He-core Masses for a Variety of sdB Models

M_{ini} ($M_\odot$)	Z_{ini}	Y_{ini}	X_{ini}	$M_{He\text{-}core}$ ($M_\odot$)	$Age_{He\text{-}flash}$ (10^9 years)	Comment
2.0	0.02	0.28	0.70	0.436	1.085	
1.2	0.02	0.28	0.70	0.464	6.212	
1.0	0.02	0.28	0.70	0.466	11.896	"Standard model"
0.9	0.02	0.28	0.70	0.467	17.142	
0.8	0.02	0.28	0.70	0.461	25.588	
0.7	0.02	0.28	0.70	No He-flash		
1.0	0.02	0.28	0.70	0.466	11.848	No winds
0.9	0.02	0.28	0.70	0.467	17.075	No winds
0.7	0.02	0.28	0.70	0.472	39.514	No winds
1.0	0.025	0.30	0.675	0.461	11.502	
1.0	0.02	0.25	0.73	0.471	14.529	
1.0	0.02	0.35	0.63	0.453	7.293	
1.0	0.01	0.26	0.73	0.471	9.976	
1.0	0.01	0.25	0.74	0.473	10.461	
1.0	0.005	0.25	0.745	0.473	7.999	

Note. The He-flash mass is approximated by the mass coordinate where the hydrogen mass fraction per cell falls below $X = 0.1$ right before the He-flash.

Our models show a growing convective core starting from $\sim$0.1 $M_\odot$ at the ZAEHB up to $\sim$0.25 $M_\odot$ at core He exhaustion. To compare our results with the convective core masses inferred from asteroseismology, we calculated time-averaged convective core masses as listed in Table 2. The $M_{ini} = 1.0\,M_\odot$, sequence average core masses are in the range of 0.17–0.18 $M_\odot$, which is substantially smaller than the values found by Van Grootel et al. (2010a, 2010b), and Charpinet et al. (2011b).

3.2. Masses of sdB Stars

According to a study of the empirical mass distribution of sdB stars (Fontaine et al. 2012), the median value of the sdB mass is $M = 0.471\,M_\odot$, with the range from 0.439 to 0.501 $M_\odot$ containing 68.3% of the stars. The maximum masses of our evolutionary sdB models lie within this range, but they are somewhat smaller than the median of the observed distribution.

The He core mass on the ZAEHB is determined by the core mass at the point when the hydrogen shell burning is quenched near the tip of the RGB, whether it is extinguished prematurely by mass stripping or by the onset of the He flash. Any mass loss occurring between the RGB tip and the ZAEHB only reduces the amount of residual hydrogen envelope; uncertainties in the mass loss rates would merely shift the sdB along the ZAEHB appropriate to its core mass.

We therefore investigated the effects on the core mass due to the interplay of initial mass, initial composition and conditions during the He flash. The results are compiled in Table 3.

Larger initial masses than 1.0 $M_\odot$ always produce smaller He cores. Initial masses smaller than 1.0 $M_\odot$ would produce larger He cores in the absence of winds, but winds reduce the mass of the He core at the He flash for lower mass stars. If the actual mass loss rates on the MS and RGB were much smaller than predicted by the Reimers formula as implemented in MESA (with a coefficient of 0.5), initial masses lower than 0.9 $M_\odot$ could result in slightly larger He core masses. However, since stars with M_{ini} smaller than about 1.0 $M_\odot$ have not had time to evolve to the RGB tip in the lifetime of the galactic disk, varying the initial mass of the MESA progenitor stars does not help to produce larger He cores than we get from our standard model.

Next we investigated the effect of different initial compositions. Table 3 shows that reducing the initial metallicity to $Z \approx 0.01$ and the helium abundances to $Y \leqslant 0.26$ would increase the He core masses to 0.471–0.473 $M_\odot$, i.e., to the median mass of the empirical mass distribution. However, since we could not realistically account for He core masses much higher than $M_{He\text{-}core} = 0.473\,M_\odot$ with composition changes alone, some additional factor would still be required to produce model sdB stars corresponding to the upper half of the observed mass distribution.

Even when sdB models are constructed to have He core masses of 0.470 $M_\odot$, or even 0.4758 $M_\odot$, the resulting ZAEHB's still appear to be a bit too far to the lower right in the $\log g - T_{eff}$ diagram. This is true for other stellar models as well as ours. According to the empirical distribution, a third of the observed points in Figure 3 should have evolved from ZAEHB's corresponding to He core masses between 0.44 $M_\odot$ and 0.47 $M_\odot$. Instead, the type II opacity ZAEHB for $M_{He\text{-}core} = 0.47\,M_\odot$ (upper/blue dashed line) appears to fall significantly below the lower envelope of the vast majority of observed points. Similarly, the upper envelope of observed points in Figures 1 and 4 seems overpopulated, especially since the evolution is much faster as the stars begin to exhaust the He in their cores.

Mixing processes in the progenitor star do influence the He core mass up to the onset of the He flash but the effect is small with current stellar evolutionary codes. We ran a few test models without atomic diffusion, starting from the pre-main-sequence, and compared them to our standard progenitor model with atomic diffusion. As seen previously by Michaud et al. (2007) and Hu et al. (2008), adopting atomic diffusion produces only a marginal increase in the He core mass of $\sim$0.0015 $M_\odot$ at the RGB tip, and consequently in the ZAEHB He core mass.

In principle the He core mass might be increased prior to the He flash by mixing processes, but within the present framework this is an arbitrary and not particularly helpful addition. For example, if convective overshoot is active during the progenitor evolution, the He core mass is enhanced by $\sim$0.0005 $M_\odot$ for an overshoot parameter of $f_{ov} = 0.02$, which is a change too small to be of significant benefit.

3.3. Observational Constraints on Initial Masses and Metallicities

Our choice of a 1.0 $M_\odot$, solar composition progenitor for most of our ZAEHB models was based on available data for sdB stars in old open clusters. Unfortunately, it is not possible to derive ages and progenitor masses for individual field sdB stars, and their current atmospheric compositions are completely independent of their original metallicities due to strong diffusion in their extremely thin envelopes. In general, since most well-studied sdB stars belong to the Galaxy's old disk population (Saffer 1991), all we know is that their progenitors must have been low mass stars less than about 10 Gyr old with metallicities greater than about 1/10 solar. More precise estimates of initial masses and metallicities can be obtained for sdB stars that are members of clusters, but only two open clusters are known to contain hot subdwarfs: NGC 6791 (5–6

sdB stars) and NGC 188 (one sdB). These also happen to be two of the oldest open clusters known, 8.3 and 6.2 Gyr, respectively (Meibom et al. 2009; Brogaard et al. 2012), as well as two of the most metal-rich, with 2.5 times solar metallicity ($Z = 0.05$) and slightly greater than solar metallicity ($Z = 0.026$; Heiter et al. 2014). NGC 6791 is a much more populous cluster, having four times as many normal He core burning red giant clump stars as NGC 188. The cluster turnoff masses, derived very precisely from eclipsing binaries, are 1.087 and 1.103 $M_{\odot}$, respectively; the ZAMS masses of the currently observed sdB progenitors would have been a few hundredths of a solar mass larger.

It turns out that there are no other well-studied clusters with ages $\gtrsim$6 Gyr and supersolar metallicities. However, it is possible to compare the statistics of sdB stars in clusters that are comparably old and more metal-poor, or somewhat younger and comparably metal-rich, or both younger and more metal-poor. While few open clusters have been definitively searched for hot stars at ultraviolet wavelengths (e.g., Zloczewski et al. 2007; Carraro et al. 2013), the presence or absence of sdBs is obvious in many open cluster color–magnitude diagrams (CMDs), wherever the blue edge of the field star distribution is significantly redder than the colors of hot subdwarfs. (Note that here we are concerned only with He core burning EHB stars, not fainter cataclysmic variables or other somewhat cooler objects sometimes suggested to be EHB candidates.)

We conducted a literature search of all well-studied old disk clusters having sufficiently deep CCD photometry to reveal faint sdB candidates and populous enough to have a distinct red giant clump (as a measure of the relative size of the cluster sample) and found the following results. There are no EHB stars in the CMDs of four old open clusters (Be 17, Be 32, Be 39, and Cr 261) with comparable ages to NGC 6791 and NGC 188 (5.5–9 Gyrs) and lower metallicities ($0.004 < Z < 0.015$). The combined red giant clump population in the CMDs of these four clusters is slightly larger than the red clump in NGC 6791 (Gozzoli et al. 1996; Bragaglia et al. 2006, 2012; Tosi et al. 2007). The CMDs of three other clusters (NGC 6819, NGC 6253, and NGC 7142) with similar metallicities to NGC 6791 and NGC 188 ($0.025 < Z < 0.05$) and younger ages (3–4 Gyr) have about the same total number of red giant clump stars as NGC 6791 and also have no EHB stars (Jeffries et al. 2013; Sandquist et al. 2013; Kaluzny et al. 2014). A sample of eight younger and more metal-poor clusters (Be 22, Be 31, Be 66, Mel 66, Tr 5, Be 29, M 67, NGC 2243; 2.5–5 Gyr, $0.003 < Z < 0.006$)(Montgomery 1993; Kaluzny 1998; Tosi et al. 2004; Di Fabrizio & Bragaglia 2005; Kaluzny et al. 2006; Andreuzzi et al. 2011; Cignoni et al. 2011; Carraro et al. 2014) with a combined red clump population more than twice that of NGC 6791, contains a total of one, still unconfirmed, EHB candidate (in Mel 66, 3.4 Gyr, $Z = 0.01$; Zloczewski et al. 2007).

To summarize, all of the confirmed sdB members of old disk clusters are found in NGC 6791 and NGC 188, both of which have supersolar metallicities and are older than 6 Gyr. Fifteen old open clusters either somewhat younger and/or more metal-poor than NGC 6791 and NGC 188 have produced, at most, a single sdB star, instead of the 20 or more such stars that would be expected if the fraction of hot subdwarfs was similar in all old disk clusters. The open cluster data suggest that lower mass, very metal-rich progenitors produce a much higher fraction of field sdB stars.

Table 3 shows that the initial masses inferred for the known sdB members of old disk clusters, 1.1–1.2 $M_{\odot}$ are consistent with observations of field sdB stars in the sense that they correspond to nearly the largest possible values of the helium core mass that could have been produced in the lifetime of the galactic disk (even if the latter are not large enough to match the observations). Significantly lower initial helium, and perhaps lower metallicities, can produce slightly larger core masses by the time of the He flash, but such low abundances are incompatible with the statistics of sdB cluster members presented above.

Most importantly, our models were evolved almost to the onset of the He flash before the envelope stripping was initiated. Assuming that sdB stars lose the last of their envelopes just as the He core flash is about to begin requires an unrealistic fine-tuning of the initial binary parameters. Instead, most sdB progenitors are expected to leave the RGB somewhat before the He core flash, when their He core masses are significantly smaller. Castellani & Castellani (1993) and D'Cruz et al. (1996) calculated that stars near the red giant tip with He core masses up to $\sim$0.02 $M_{\odot}$ less than the He flash core mass can lose their envelopes and still become EHB stars.

Although the He core masses of our standard MESA sdB models are already too small compared to observations, it is clear that more realistic assumptions would reduce the ZAEHB He core masses even further, increasing the discrepancy with observations.

3.4. A Solution from Nuclear Astrophysics?

It might be thought that our inability to produce higher He core masses is related to the net rates of the helium burning reactions which are used as defaults in MESA, indicating that these rates might need revision.

The mass at degenerate ignition is essentially a measure of the peak temperature, and insensitive to other parameters. In turn, the temperature at thermal runaway is sensitive to the effective reaction rate, including both nuclear and electron screening effects. Hoyle (1954) used this physics plus the core mass–luminosity relation to infer the existence of an excited state in ^{12}C; see Section 8.1, Arnett (1996), for details. We expect a slightly lower effective rate to give a later helium flash, allowing the core to grow larger. Iliadis (2007) (Section 5.3.1) has reviewed the experimental situation regarding the rates of helium burning reactions. The triple-alpha reaction is not directly measured, but is thought to be reliably estimated ($\pm$35%) by indirect means for normal, non-degenerate conditions. The $^{12}C(\alpha,\gamma)^{16}O$ reaction is notorious for its experimental difficulty, but must track the triple-alpha rate to avoid significant nucleosynthesis consequences.

To test the sensitivity of core mass to reaction rate, we performed a numerical experiment in which we simply lowered the effective nuclear reaction rates for our stellar progenitor model. We decreased the effective nuclear reaction rates for the triple-α process and the nitrogen reactions by a factor of 4, which led to a He-core mass of 0.473 $M_{\odot}$ (factor of 2: 0.469 $M_{\odot}$) for the $M_{\rm ini} = 1.0\,M_{\odot}$ model, bringing the He-core mass slightly above the median of the sdB mass distribution. These arbitrary changes are three times the estimated 3σ error, and seem to be an very unlikely resolution of the discrepancy in He core masses of sdB stars.

Table 4
Global Properties for sdB Models with Different Input Physics

Model Physics	sdB Lifetime (10^6 years)	Average $M_{cc}(M_\odot)$
Default (OPAL I, no diffusion)	90.7	0.105
Basic (OPAL II, no diffusion)	77.8	0.105
Basic + $f_{ov} = 0.02$	176.8	0.157
Standard (OPAL II, with diffusion)	146.8	0.172
Standard + $f_{ov} = 0.02$	174.6	0.157
Standard + rad. levitation	146.9	0.168

4. CONVECTIVE CORES OF sdB STARS

Using our standard set of input physics, including the well described set of physical processes causing atomic diffusion, we found that our time-averaged convective core masses are too small in comparison to the data inferred from asteroseismology. A combination of type II opacities plus atomic diffusion is clearly necessary, although insufficient. A further increase of the average convective core mass of about 0.04–0.09 $M_\odot$ is needed for agreement with the values found by Van Grootel et al. (2010a, 2010b) and Charpinet et al. (2011b).

The convective core size is mainly determined by the convective and diffusive mixing processes during the evolution of the sdB star. For our standard models, we used the Schwarzschild criterion to determine the convective boundary and the MLT picture of convection.

In the following sections, we further investigate the different input physics options available in MESA to illustrate how the interplay of opacities, diffusion, and overshoot affect the convective core growth, and thus the sdB lifetime, as well as the position in the $\log g - T_{\rm eff}$ diagram.

4.1. Direct Comparison of Different Input Physics

We compared six different sdB models, all having the same standard $M_{\rm ini} = 1.0\,M_\odot$ progenitor model and $M_{\rm new} = 0.48\,M_\odot$, using different options for the input physics as specified in Table 4. The default model uses most of the MESA default input physics, including OPAL type I opacities and no atomic diffusion. The basic model uses the OPAL type II opacities and again no atomic diffusion. The third model in this comparison adds convective overshoot to the basic model. Our standard sdB model has the input physics summarized in Table 1. The fifth model adds convective overshoot to the standard model, and the last model shows the affect of radiative levitation.[3]

The results for the convective core masses are shown in Figure 5. The default and the basic model both have a constant convective core mass of 0.1 $M_\odot$ throughout the sdB lifetime, which is therefore significantly shorter than for the standard model. Adding convective overshoot with $f_{ov} = 0.02$ to the basic model allows the convective core to grow from a value of about 0.13 $M_\odot$ to 0.16 $M_\odot$. From then on, the convective core size in the basic $+ f_{ov}$ model remains roughly constant, but the convective boundary shows rapid irregular fluctuations probably related to inadequacies in the formulation of the overshoot algorithm. The sdB lifetime for this model is extended by about a factor of two compared to the default and the basic model.

The standard model also produces a steadily growing convective core up to a mass of $\approx 0.25\,M_\odot$ at He core exhaustion, as described in Section 3.1. This is our only model in which the increase in the convective core mass is monotonic and smooth. The sdB lifetime is ~50 Myr longer than for the default and basic models, in full agreement with the results of Bloemen et al. (2014).

A default model with convective overshoot (not listed in the table) showed that the current MESA overshoot algorithm simply forces the size of the convective core to have a larger constant value, whereas the combined effect of using type II opacities and either overshoot (basic + f_{ov}) or atomic diffusion (standard) is to cause core growth.

When overshoot is added to the standard model, we see the same behavior discussed above for the basic model with overshoot, including the same rapid fluctuations, except that the maximum convective core size and the lifetime are both larger.

Adding radiative levitation slightly decreases the average convective core mass of our standard model because of the sawtooth behavior seen in Figure 5. It has a negligible effect on the sdB lifetime. We encountered the sawtooth behavior in many of our other standard models (i.e., without radiative levitation). The convection zone grows and collapses periodically in these models.

We believe this is not a numerical artefact but is rather a consequence of the model physics. The effect is reminiscent of He-flash models by Moćak et al. (2008, 2009). It seems to be strongly dependent on the different model parameters, especially the new mass after stripping off the envelope. This behavior changes the profile of the helium, carbon, and oxygen abundances as a function of time, compared to a smooth curve, although it does not help to explain the discrepancies between the convective core masses of our models and the ones inferred from asteroseismology.

Figure 6 shows the evolutionary tracks of five of the six models compared to sdB observational data. When type II opacities are used (basic model; black circles) instead of type I opacities (default model; open circles) the evolutionary paths shift to higher temperatures and very slightly higher gravities. The most significant difference is the evolution to much lower gravities caused by the convective core growth, due to the combination of type II opacities and either overshoot in the basic model or diffusion in the standard model (black squares). The resulting tracks extend high enough to explain a majority of the observed points. The standard model plus radiative levitation (gray diamonds; red in the online version) gives a similar result. Adding overshoot to either the basic model (not plotted) or the standard model (gray squares; blue in the online version) also turns out fairly similar, except for the suspicious looping behavior toward the end of the He core burning in Figure 6, corresponding to the large spikes in Figure 5. (The tracks of the two models with convective overshoot are so similar that for clarity we only show the standard model with overshoot.)

4.2. Achieving Larger Convective Cores with Convective Overshoot

Although we see erratic behavior when convective overshoot is added to any model computed with type II opacities, we nonetheless calculated a few models with varying overshoot

[3] Radiative levitation in this model makes use of OPAL Project opacities (Badnell et al. 2005), which include additional data for iron group elements.

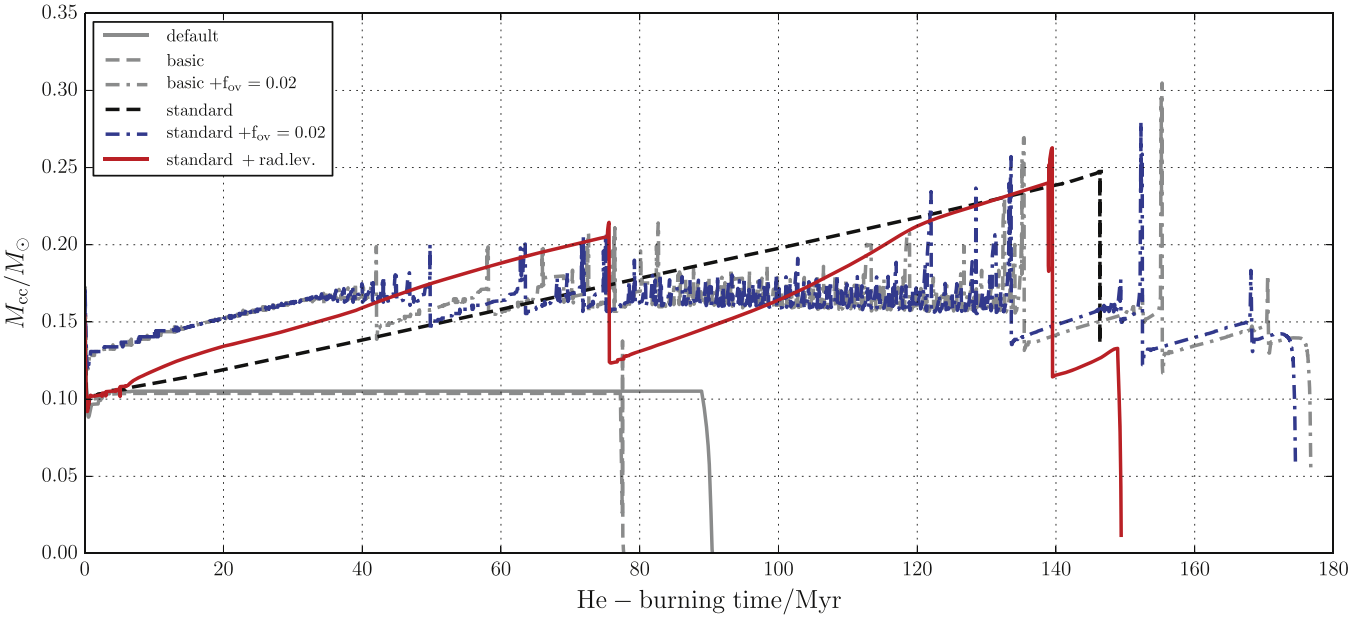

Figure 5. Convective cores as a function of time, with different input physics. The largest cores result from a combination of type II opacities and either overshoot or atomic diffusion, which conspire to induce core growth. Large values for the overshoot parameter do not produce core growth, just larger cores. The rapid fluctuations in the models with overshoot suggest that the mixing algorithm experiences numerical instabilities at the boundary. The model with radiative levitation shows a sawtooth curve that we also find in some of our other standard models without radiative levitation. The sawtooth is caused by the convection zone growing and collapsing periodically.

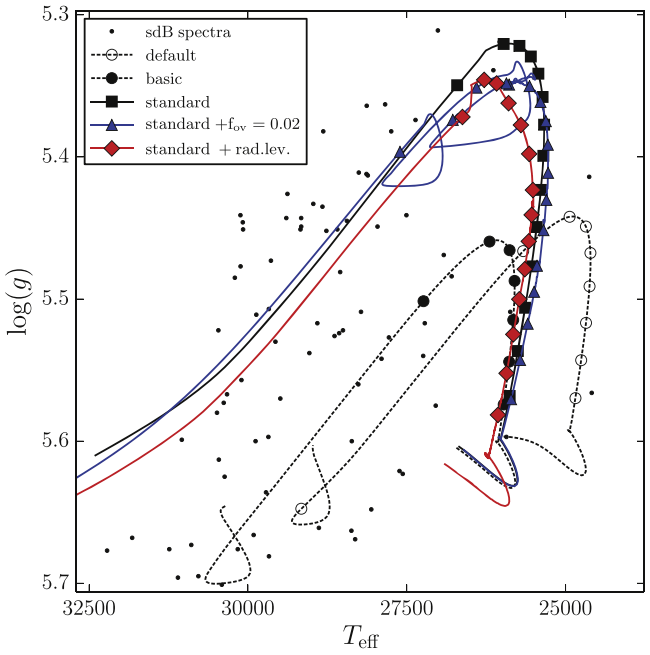

Figure 6. Evolutionary tracks starting from the same standard initial model, but with different input physics. The sdB observational data are shown as single symbols and the evolutionary tracks are shown as symbols connected by lines. (The basic model with overshoot was not plotted, since it is indistinguishable from the standard model with overshoot.) As in Figure 5, the most significant change results from core growth due to the combination of type II opacities and either overshoot or atomic diffusion.

parameters to investigate whether a sufficiently large overshoot parameter in the current implementation would bridge the discrepancy in convective core size between our stellar models and asteroseismology.

Table 5 lists the results of two model sequences with varying amounts of convective overshoot, as implemented in MESA.

Table 5
Properties for sdB Models with Additional Overshoot

	Standard Model (OPAL II and Diffusion)		Basic Model (OPAL II, No Diffusion)	
Overshoot Parameter f_{ov}	sdB Lifetime (10^6 years)	Convective Core Mass $M_{cc}(M_\odot)$	sdB Lifetime (10^6 years)	Convective Core Mass $M_{cc}(M_\odot)$
No overshoot	146.8	0.172	77.8	0.105
0.01	194.8	0.149	179.4	0.152
0.02	174.6	0.157	176.8	0.157
0.04	176.2	0.179	174.98	0.179
0.08	170.3	0.227	170.2	0.227
0.10	179.3	0.252	179.2	0.252

Except for the value of the overshoot parameter, these model sequences are the same as the basic and standard models in Table 4. They start from the same progenitor model evolved with standard input physics ($M_{ini} = 1.0\,M_\odot$, $M_{new} = 0.48\,M_\odot$).

An increase in the overshoot parameter, f_{ov}, directly affects the extent of the convective core. To achieve convective cores as large as those determined by Van Grootel et al. (2010a, 2010b) and Charpinet et al. (2011b), the overshoot parameter must be greater than 0.08. For reference, we note that overshoot parameters $f_{ov} \sim 10^{-5}$–10^{-4} have been used for $3\,M_\odot$ stars and overshoot parameters $f_{ov} \sim 10^{-3}$–10^{-2} for $1.5\,M_\odot$ stars (Paxton et al. 2013). Herwig (2000) suggested $f_{ov} \sim 0.016$ for stellar interiors in order to reproduce the models of Schaller et al. (1992).

We have to increase the overshoot parameter by at least a factor of five to reproduce values close to the results of Grootel et al. and Charpinet et al. even in the presence of atomic diffusion in our standard model. The fact that the overshoot parameter must be varied by orders of magnitude in different

types of stars underscores the physical inadequacy of the current treatment of overshooting.

It is interesting that convective overshoot seems to hinder the convective core growth that occurs as a result of atomic diffusion and type II opacities in our standard model. Table 5 shows that overshoot parameters of 0.01–0.02 produce smaller average convective core masses than the standard model with no overshoot. Larger convective core masses are achieved only for $f_{ov} \geqslant 0.04$. It appears that overshoot interacts in an unexpected way with diffusion as well as with type II opacities.

The overshoot algorithm increases core sizes by increasing the importance of the numerical diffusion term (Eggleton 1972), which in turn flattens the composition gradients. Smaller gradients make atomic diffusion weaker; actually, overshoot should enhance atomic diffusion.

5. CONCLUSION

MESA is an excellent software environment to explore the implications of numerical experiments, and to find inadequacies in our theoretical ideas about how stars evolve.

Our MESA sdB models reproduce the general properties of the ZAEHB and the characteristic hook shape of the helium core burning evolutionary path. We have demonstrated that MESA is fully capable of recreating previous theoretical EHB results, e.g., the position of the tracks in the $\log g - T_{\rm eff}$ plane and the model timescales (Charpinet et al. 2002; Bloemen et al. 2014), as long as we use Type II opacities and start with the same value for the He-core mass on the ZAEHB.

However, although we are able to produce structures which are consistent with the asteroseismology of sdB stars, *we cannot evolve to these conditions with plausible parameters for standard stellar evolution.* Our largest total sdB masses are smaller than the median mass of the empirical sdB mass distribution. More importantly, the computed helium burning cores are smaller than inferred by observation. This is an error in convective mixing in the deep interior, far from any superadiabatic region in the envelope. It cannot be blamed on MLT alone, and is *likely to be related to the treatment of the convective boundary.*

A clue for the solution of this problem comes from 3D simulations of stellar convection having sufficient resolution to show turbulent flow (Viallet et al. 2013). These simulations provide a closure for the Reynolds averaged Navier–Stokes analysis, which in turn suggests approximations which would allow this behavior to be implemented in a stellar evolutionary code. They do not require calibration to astronomical data. See W. D. Arnett et al. (2015, in preparation) for details; here we summarize a few features relevant to the sdB problem. A robust feature of these simulations is the development of a boundary layer between convective and nonconvective regions, in which the radial flow is turned so that convection stays within the convective region. This braking layer is subadiabatic and well mixed so that mixing extends beyond the radius defined by the Schwarzschild criterion; "extra mixing" is required, and not an option. The braking layers are narrow, with a width which depends upon the stiffness of the stable layer and the velocity of the flow; stiff boundaries and slow flow have narrower braking layers. The bulk of the convective region (away from the convective boundary) is moderately well described by MLT, a fact which, along with the free parameter, explains its level of success and enduring popularity.

It appears that convection as presently implemented in stellar evolution codes is inadequately accurate for precise tests, such as those imposed by asteroseismology. We also note that such a boundary modification would tend to shift the standard solar model toward the Asplund abundances (Asplund et al. 2009). The inferred core sizes of the sdB stars and the 3D simulations suggest a consistent picture may be obtained with the introduction of more physically consistent boundary conditions into stellar evolutionary codes.

This work was supported in part by the NSF Award 1107445 at the University of Arizona. We thank Stéphane Charpinet, Gilles Fontaine, Conny Aerts, Steven Bloemen, and John Lattanzio for helpful and constructive discussions, and G. Bono for interesting questions.

REFERENCES

Andreuzzi, G., Bragaglia, A., Tosi, M., & Marconi, G. 2011, MNRAS, 412, 1265
Arnett, D. 1996, Supernovae and Nucleosynthesis (Princeton, NJ: Princeton Univ. Press)
Asplund, M., Grevesse, N., Sauval, A. J., & Scott, P. 2009, ARA&A, 47, 481
Badnell, N. R., Bautista, M. A., Butler, K., et al. 2005, MNRAS, 360, 458
Baran, A. S., Reed, M. D., Stello, D., et al. 2012, MNRAS, 424, 2686
Bergeron, P., Wesemael, F., Michaud, G., & Fontaine, G. 1988, ApJ, 332, 964
Blöcker, T. 1995, A&A, 297, 727
Bloemen, S., Hu, H., Aerts, C., et al. 2014, A&A, 569, A123
Böhm-Vitense, E. 1958, ZA, 46, 108
Bragaglia, A., Gratton, R. G., Carretta, E., et al. 2012, A&A, 548, A122
Bragaglia, A., Tosi, M., Carretta, E., et al. 2006, MNRAS, 368, 1971
Bressan, A., Girardi, L., Marigo, P., Rosenfield, P., & Tang, J. 2015, APSS, 39, 25
Brogaard, K., VandenBerg, D. A., Bruntt, H., et al. 2012, A&A, 543, A106
Carraro, G., Buzzoni, A., Bertone, E., & Buson, L. 2013, AJ, 146, 128
Carraro, G., de Silva, G., Monaco, L., Milone, A. P., & Mateluna, R. 2014, A&A, 566, A39
Cassisi, S., Potekhin, A. Y., Pietrinferni, A., Catelan, M., & Salaris, M. 2007, ApJ, 661, 1094
Castellani, M., & Castellani, V. 1993, ApJ, 407, 649
Charpinet, S., Fontaine, G., Brassard, P., & Dorman, B. 2000, ApJS, 131, 223
Charpinet, S., Fontaine, G., Brassard, P., & Dorman, B. 2002, ApJ, 140, 469
Charpinet, S., Fontaine, G., Brassard, P., et al. 1997, ApJL, 483, L123
Charpinet, S., Fontaine, G., Brassard, P., et al. 2011a, Natur, 480, 496
Charpinet, S., Van Grootel, V., Fontaine, G., et al. 2011b, A&A, 530, A3
Charpinet, S., Van Grootel, V., Reese, D., et al. 2008, A&A, 489, 377
Chayer, P., Fontaine, G., Fontaine, M., et al. 2004, Ap&SS, 291, 359
Cignoni, M., Beccari, G., Bragaglia, A., & Tosi, M. 2011, MNRAS, 416, 1077
Cox, J. P., & Giuli, R. T. 1968, Principles of Stellar Structure (New York: Gordon and Breach)
D'Cruz, N. L., Dorman, B., Rood, R. T., & O'Connell, R. W. 1996, ApJ, 466, 359
Di Fabrizio, L., Bragaglia, A., Tosi, M., & Marconi, G. 2005, MNRAS, 359, 956
Dorman, B., & Rood, R. T. 1993, ApJ, 409, 387
Dorman, B., Rood, R. T., & O'Connell, R. W. 1993, ApJ, 419, 596
Eggleton, P. 1972, MNRAS, 156, 361
Fontaine, G., Brassard, P., Charpinet, S., et al. 2003, ApJ, 597, 518
Fontaine, G., Brassard, P., Charpinet, S., et al. 2012, A&A, 539, A12
Fontaine, G., Brassard, P., Charpinet, S., & Chayer, P. 2006a, MmSAI, 77, 49
Fontaine, G., & Chayer, P. 1997, in Third Conf. on Faint Blue Stars, ed. A. G. D. Philip, J. W. Liebart, & R. A. Saffer (Schenectady, NY: L. Davis Press), 169
Fontaine, G., Green, E. M., Chayer, P., et al. 2006b, BaltA, 15, 211
Freytag, B., Ludwig, H.-G., & Steffan, M. 1996, A&A, 313, 497
Gozzoli, E., Tosi, M., Marconi, G., & Bragaglia, A. 1996, MNRAS, 283, 66
Green, E. M., Fontaine, G., Hyde, E. A., For, B.-Q., & Chayer, P. 2008, Hot Subdwarf Stars and Related Objects, 392, 75
Green, E. M., Fontaine, G., Reed, M. D., et al. 2003, ApJL, 583, L31
Green, E. M., Guvenen, B., O'Malley, C. J., et al. 2011, ApJ, 734, 59
Han, Z., Podsiadlowski, P., Maxted, P. F. L., & Marsh, T. R. 2003, MNRAS, 341, 669

Han, Z., Podsiadlowski, P., Maxted, P. F. L., Marsh, T. R., & Ivanova, N. 2002, MNRAS, 336, 449
Heber, U. 1986, A&A, 155, 33
Heber, U., Reid, I., & Werner, K. 2000, A&A, 363, 198
Heiter, U., Soubiran, C., Netopil, M., & Paunzen, E. 2014, A&A, 561, A93
Herwig, F. 2000, A&A, 360, 952
Hoyle, F. 1954, ApJS, 1, 121
Hu, H., Dupret, M., Aerts, C., et al. 2008, A&A, 490, 243
Hu, H., Glebbeek, E., Thoul, A. A., et al. 2010, A&A, 511, A87
Hu, H., Nelemans, G., Aerts, C., & Dupret, M.-A. 2009, A&A, 508, 869
Hu, H., Tout, C. A., Glebbeek, E., & Dupret, M.-A. 2011, MNRAS, 418, 195
Iglesias, C., & Rogers, F. 1993, ApJ, 412, 752
Iglesias, C., & Rogers, F. 1996, ApJ, 464, 943
Iliadis, C. 2007, Nuclear Physics of Stars (Wenheim: Wiley-VCH Verlag)
Jeffries, M. W., Sandquist, E. L., Mathieu, R. D., et al. 2013, AJ, 146, 58
Kaluzny, J. 1998, A&AS, 133, 25
Kaluzny, J., Rozyczka, M., Pych, W., & Thompson, I. B. 2014, AcA, 64, 77
Kaluzny, J., Krzeminski, W., Thompson, I. B., & Stachowski, G. 2006, AcA, 56, 51
Kilkenny, D., Koen, C., O'Donoghue, D., & Stobie, R. S. 1997, MNRAS, 285, 640
Landau, L. D., & Lifshitz, E. M. 1959, Fluid Mechanics (Oxford: Pergamon Press)
Langer, N., Fricke, K. J., & Sugimoto, D. 1983, AA&A, 126, 207
Meibom, S., Grundahl, F., Clausen, J. V., et al. 2009, AJ, 137, 5086
Mengel, J. G., Norris, J., & Gross, P. G. 1976, ApJ, 204, 488
Michaud, G. 1970, ApJ, 160, 641
Michaud, G. 1991, AnPhy, 16, 481
Michaud, G., Bergeron, P., Wesemael, F., & Fontaine, G. 1985, ApJ, 299, 741
Michaud, G., Richer, J., & Richard, O. 2007, ApJ, 670, 1178
Michaud, G., Richer, J., & Richard, O. 2008, ApJ, 675, 1223
Michaud, G., Richer, J., & Richard, O. 2011, A&A, 529, 60
Miller Bertolami, M. M., Althaus, L. G., Unglaub, K., et al. 2008, A&A, 491, 253
Moćak, M., Müller, E., Weiss, A., & Kifonidis, K. 2008, A&A, 490, 265
Moćak, M., Müller, E., Weiss, A., & Kifonidis, K. 2009, A&A, 501, 659
Montgomery, K., Marschall, L. A., & Janes, K. A. 1993, AJ, 106, 181
Østensen, R. H., Degroote, P., Telting, J. H., et al. 2012, ApJL, 753, L17
Pablo, H., Kawaler, S. D., Reed, M. D., et al. 2012, MNRAS, 422, 1343
Paxton, B., Bildsten, L., Dotter, A., et al. 2011, ApJS, 192, 3
Paxton, B., Cantiello, M., Arras, P., et al. 2013, ApJS, 208, 4
Randall, S. K., Green, E. M., Van Grootel, V., et al. 2007, A&A, 476, 1317
Reimers, D. 1975, MSRSL VIII, 369
Saffer, R. A. 1991, PhD thesis, Univ. Arizona, Tucson
Saffer, R. A., Bergeron, P., Koester, D., & Liebert, J. 1994, ApJ, 432, 351
Sandquist, E. L., Shetrone, M., Serio, A. W., & Orosz, J. 2013, AJ, 146, 40
Schaller, G., Schaerer, D., Meynet, G., & Maeder, A. 1992, A&AS, 96, 269
Schuh, S., Huber, J., Dreizler, S., et al. 2006, A&A, 445, 31
Sweigart, A. V. 1987, ApJS, 65, 95
Tosi, M., Bragaglia, A., & Cignoni, M. 2007, MNRAS, 378, 730
Tosi, M., Di Fabrizio, L., Bragaglia, A., Carusillo, P. A., & Marconi, G. 2004, MNRAS, 354, 225
Van Grootel, V., Charpinet, S., Fontaine, G., et al. 2008, A&A, 488, 685
Van Grootel, V., Charpinet, S., Brassard, P., Fontaine, G., & Green, E. M. 2013, A&A, 553, A97
Van Grootel, V., Charpinet, S., Fontaine, G., Green, E. M., & Brassard, P. 2010a, A&A, 524, A63
Van Grootel, V., Charpinet, S., Fontaine, G., et al. 2010b, ApJL, 718, L97
Viallet, M., Meakin, C., Arnett, D., & Mocák, M. 2013, ApJ, 769, 1
Zloczewski, K., Kaluzny, J., Krzeminski, W., Olech, A., & Thompson, I. B. 2007, MNRAS, 380, 1191